

Apparent Loss and Hypertrophy of Interneurons in a Mouse Model of Neuronal Ceroid Lipofuscinosis: Evidence for Partial Response to Insulin-Like Growth Factor-1 Treatment

Jonathan D. Cooper,¹ Anne Messer,² Andrew K. Feng,¹ Jane Chua-Couzens,¹ and William C. Mobley¹

¹Department of Neurology and Neurological Sciences and the Program in Neuroscience, Stanford University, Stanford, California 94305-5489, and ²Wadsworth Center, New York State Department of Health, Albany, New York 12201-2002

The neuronal ceroid lipofuscinoses (NCL) are progressive neurodegenerative disorders with onset from infancy to adulthood that are manifested by blindness, seizures, and dementia. In NCL, lysosomes accumulate autofluorescent proteolipid in the brain and other tissues. The *mnd/mnd* mutant mouse was first characterized as exhibiting adult-onset upper and lower motor neuron degeneration, but closer examination revealed early, widespread pathology similar to that seen in NCL. We used the autofluorescent properties of accumulated storage material to map which CNS neuronal populations in the *mnd/mnd* mouse show NCL-like pathological changes. Pronounced, early accumulation of autofluorescent lipopigment was found in subpopulations of GABAergic neurons, including interneurons in the cortex and hippocampus. Staining for phenotypic markers nor-

mally present in these neurons revealed progressive loss of staining in the cortex and hippocampus of *mnd/mnd* mice, with pronounced hypertrophy of remaining detectable interneurons. In contrast, even in aged mutant mice, many hippocampal interneurons retained staining for glutamic acid decarboxylase. Treatment with insulin-like growth factor-1 partially restored interneuronal number and reduced hypertrophy in some subregions. These results provide the first evidence for the involvement of interneurons in a mouse model of NCL. Moreover, our findings suggest that at least some populations of these neurons persist in a growth factor-responsive state.

Key words: neuronal ceroid lipofuscinosis; *mnd/mnd*; hippocampal and cortical interneurons; GABAergic; neurodegeneration; IGF-1

The neuronal ceroid lipofuscinoses (NCLs) are progressive, fatal neurodegenerative disorders of unknown pathogenesis with onset ranging from infancy to adulthood. Childhood forms are manifested by blindness, seizures, and dementia (Dyken, 1988; Goebel, 1995). Collectively, these disorders represent the most common inherited neurodegenerative storage disorder of childhood with an incidence of 1 in 12,500 live births (Goebel, 1995). The NCLs have traditionally been divided into four main types (Dyken, 1988; Goebel, 1995), although variant forms are reported (Dyken, 1988; Santavuori et al., 1991; Dyken and Wisniewski, 1995). In recent studies, genes have been discovered for the infantile form (*CLN1*) (Haltia-Santavuori disease) (Vesa et al., 1995), late infantile form (*CLN2*) (Jansky-Bielschowsky disease) (Sleat et al., 1997), juvenile form (*CLN3*) (Batten disease or Spielmeyer-Sjogren disease) (The International Batten Disease Consortium, 1995), and Finnish variant of the late infantile form (*CLN5*) (Savukoski et al., 1998). The gene for Kufs disease (*CLN4*), an adult-onset form of the disorder, awaits definition.

The characteristic feature of NCL pathology is the lysosomal

accumulation of autofluorescent proteolipid in the brain and other tissues (Koenig, 1964; Haltia et al., 1973; Dyken, 1988; Goebel, 1995). Ultrastructurally, these electron-dense accumulations exhibit granular, curvilinear, or fingerprint-like appearances that are characteristic for each form of NCL (Santavuori, 1988; Goebel, 1995, 1997). Biochemical studies of these deposits in *CLN2*, *CLN3*, and *CLN4* have shown that the major protein component is subunit *c* of the mitochondrial ATPase (Hall et al., 1991; Kominami et al., 1992; Palmer et al., 1992). In *CLN1*, deposits are largely composed of saposins A and D (Tyynelä et al., 1993). The molecular mechanisms by which mutations in the *CLN* genes lead to pathophysiology are unidentified.

The development of an animal model that recapitulates the clinical and pathological features of NCL represents an initial step toward discovering underlying disease mechanisms and testing potential treatment strategies. The *mnd/mnd* mouse was first characterized as a spontaneous autosomal mutant that exhibits adult-onset upper and lower motor neuron degeneration (Messer and Flaherty, 1986; Messer et al., 1987). Closer examination revealed pathology similar to that seen in NCL (Bronson et al., 1993; Mazurkiewicz et al., 1993; Pardo et al., 1994). The mice exhibit progressive retinopathy leading to blindness (Messer et al., 1993) and early, widespread accumulation of subunit *c* and autofluorescent lipopigment in many tissues (Bronson et al., 1993; Messer and Plummer, 1993; Pardo et al., 1994). Thus, although mapping data indicate that *mnd* is not one of the identified genes mutated in the NCLs (Messer et al., 1992), the *mnd/mnd* mouse does model certain clinical and pathological features of these disorders.

In this study of the *mnd/mnd* mouse, we have used the autofluorescent properties of accumulated lipopigment to show which

Received Oct. 27, 1998; revised Dec. 18, 1998; accepted Jan. 14, 1999.

This work was supported by National Institutes of Health Grant NS29110 (A.M.), The Remy foundation (J.D.C.), The Batten's Disease Support and Research Association, The Natalie Fund, and the Children's Brain Diseases Foundation (W.C.M., A.M.). IGF-1 was provided by Dr. Nicola Neff of Cephalon Inc. We thank Drs. D. N. Palmer and S. Baekkeskov for the gifts of antisera, and Drs. Serge Marty, Hannah Mitchison, and Alison Barnwell for critical review of this manuscript. We thank Kevin Manley for expert maintenance of the *mnd* mouse colony. We also thank Dr. Eric Beattie for assistance in obtaining and processing data via confocal microscopy.

Correspondence should be addressed to Dr. Jonathan D. Cooper, Department of Neurology and Neurological Sciences, Medical Sciences Laboratory Surge Building, Room P220, MC 5489, Stanford University, 1201 Welch Road, Stanford, CA 94305-5489. E-mail: cerebus@leland.stanford.edu

Copyright © 1999 Society for Neuroscience 0270-6474/99/192556-12\$05.00/0

neuronal populations show NCL-like pathological changes and examined the onset and progression of pathological changes. We report on the results of treating *mnd/mnd* mice with insulin-like growth factor-1 (IGF-1), a neurotrophic factor, to attempt to halt the progression of degenerative changes.

MATERIALS AND METHODS

Animals

Mnd/mnd mice on a C57BL/6J (B6) background were bred in the colonies maintained at the David Axelrod Institute, New York State Department of Health, Albany, NY, and transferred to the University of California at San Francisco (UCSF) animal facility at 4–8 months of age. An additional group of 2-month-old animals were perfused at the David Axelrod Institute, as described below, and their brains were sent to UCSF on dry ice. All animal procedures were approved by the Institutional Animal Care and Use Committees.

Histological processing

The CNS of female *mnd/mnd* B6 and age-matched control (+/+) B6 mice were examined at ages up to 9-months-old ($n = 5$ at each age), the maximum age to which mutant mice survived in our colony. For histological analysis, female *mnd/mnd* B6 and age-matched control (+/+) B6 mice were deeply anesthetized with pentobarbitone and transcardially perfused with vascular rinse (0.8% NaCl, 0.025% KCl, 0.005% CaCl₂, 0.05% NaHCO₃, and 100 mM NaHPO₄) followed by a freshly made and filtered solution of 4% paraformaldehyde and 0.2% picric acid in 100 mM phosphate buffer, pH 7.4. Brains were subsequently removed and post-fixed for six hr at 4°C in the same fixative before cryoprotection at 4°C in a solution of 30% sucrose in Tris-buffered saline (TBS; 40 mM Tris and 0.7% NaCl in 10 mM phosphate buffer, pH 7.8) containing 0.05% Na₂S₂O₈ frozen coronal sections were collected in TBS–azide buffer and stored at 4°C before Nissl or immunohistochemical staining, which normally occurred on the same day as cutting.

Unbiased estimates of regional volume

For each brain, a one-in-six series of 40 μ m sections through the entire rostrocaudal extent of the CNS was mounted on glass microscope slides, lightly counterstained with cresyl violet and dehydrated through graded concentrations of ethanol, cleared in xylene, and coverslipped with DPX (BDH Chemicals, Poole, UK). Sections were visualized with an MCID image analysis system linked to a CCD camera with a 35 mm lens, and unbiased estimates of the volume of brain regions were made using Cavalieri's (1966) method, by counting the number of points of a randomly superimposed sampling grid that fell over each structure.

Mapping of affected cells

For each brain, a one-in-six series of 40 μ m sections through the entire rostrocaudal extent of the CNS was mounted on glass microscope slides, air-dried, and coverslipped with a laboratory-derived aqueous mounting medium. Sections were viewed by conventional fluorescence microscopy using standard filtersets for the detection of FITC and rhodamine. A parallel series of sections was stained with a polyclonal antiserum raised against subunit *c* of sheep mitochondrial ATPase (a kind gift of Dr. D. Palmer, Palmerston, New Zealand). Selected sections through CNS regions were also stained by conventional immunofluorescence techniques (see below) using Texas red-conjugated secondary antisera to reveal the presence of antigens that colocalize with GABA. As detailed below, confocal microscopy was used to reveal the colocalization of these phenotypic markers with autofluorescent lipopigment.

Immunohistochemical staining

For each brain, a one-in-six series of sections through the hippocampal formation and cortical mantle were stained according to standard immunohistochemical protocols to reveal the distribution of neurons expressing either parvalbumin (PV), calbindin (Cb), somatostatin-14 (SOM), or glutamic acid decarboxylase (GAD). A one-in-three series of 40 μ m sections through the septal region was also stained to reveal the presence of neurons expressing PV or choline acetyltransferase (ChAT).

Immunoperoxidase staining. Briefly, sections were incubated in 1% H₂O₂ in TBS (0.04 M Tris, 0.7% NaCl, and 0.01 M sodium phosphate buffer), rinsed in TBS, and blocked for 20 min with 15% appropriate

normal serum before overnight incubation at 4°C with a solution of primary antibody [polyclonal rabbit anti-PV, Swant, Bellinzona, Switzerland, 1:5000; polyclonal rabbit anti-calbindin, Swant, 1:20,000; polyclonal rabbit anti-SOM, Chemicon, Temecula, CA, 1:1000; affinity-purified goat anti-ChAT, Chemicon, 1:1000; polyclonal rabbit anti-sheep subunit *c*, 1:1000; affinity-purified rabbit anti-GAD (serum 1701), a generous gift of Dr. S. Baekkeskov, University of California, San Francisco, 1:2000] diluted in TBS with 10% normal serum, and 0.3% Triton X-100. Sections were subsequently rinsed with TBS, incubated for 2 hr in secondary antiserum, (biotinylated donkey anti-goat IgG or biotinylated goat anti-rabbit IgG; Vector Laboratories, Burlingame, CA) diluted 1:1000 in TBS with 10% normal serum, and 0.3% Triton X-100, and washed with TBS before incubation for 2 hr in avidin–biotin–peroxidase complex in TBS (Vectastain; Vector Laboratories). Finally, sections were rinsed with TBS and incubated for ~10 min in the dark with 0.05% diaminobenzidine tetrahydrochloride and 0.001% H₂O₂ in TBS. The staining reaction was stopped by adding excess ice-cold TBS. Sections were mounted, air-dried, cleared in xylene, and coverslipped with DPX (BDH Chemicals).

Immunofluorescence staining. Selected sections through the septum, hippocampal formation, and entorhinal cortex were stained by conventional immunofluorescence techniques to reveal the presence of ChAT-, PV-, Cb-, and SOM-expressing neurons. Briefly, sections were incubated in primary antisera as above before rinsing in TBS followed by incubation in secondary antiserum (Texas red-conjugated donkey anti-goat or donkey anti-rabbit; Jackson ImmunoResearch, West Grove, PA) diluted 1:500 in TBS with 10% normal serum, and 0.3% Triton X-100 and washed with TBS before being mounted on glass microscope slides, air-dried, and coverslipped with a laboratory-derived aqueous mounting medium. The extent of colocalization of lipopigment and phenotypic markers was determined by confocal microscopy using a Bio-Rad (Hercules, CA) MRC 1000 confocal microscopy system linked to a Zeiss Axiovert microscope.

Measurements of detectable neuronal number and cross-sectional area

Septal region. The number of PV-expressing GABAergic neurons and ChAT-expressing cholinergic neurons in the septal region were determined in an unbiased manner using the optical disector method in combination with the Cavalieri method for estimating reference volume (West and Gundersen, 1990). The first section in each series was chosen randomly followed by every third section thereafter, with a total of 10 sections per animal. Cells were sampled using a disector frame taped to the monitor screen; cells were counted if they contained a nucleus that fell within the disector frame under a 100 \times objective (NA 1.32). The cross-sectional area of each counted profile was then measured as described. All counts were performed in a double-blind manner without previous knowledge of the genotype by the person performing sectioning or counting.

Entorhinal cortex and hippocampal formation. Counts of detectable PV-expressing neurons were made in the five most rostral sections of a one-in-six series of sections through layers II and IV of the entorhinal cortex and of PV-, Cb-, SOM-, and GAD-positive neurons in the five most rostral sections of a similar series through the hippocampal formation. The number of positive neurons was determined under a 25 \times objective, counting only neurons with a clearly identifiable nucleus. This value was expressed as the number of detectable neurons per section and corrected by the method of Abercrombie (1946). The same sections were examined under a 100 \times objective, and measurements of cross-sectional area were made with an MCID image analysis system linked to a CCD camera for at least 100 PV-positive interneurons in the entorhinal cortex and at least 50 positive neurons for each antigen in the hippocampal formation. These results were presented in the form of cell-size distribution histograms using a bin size of 20 μ m. All measurements were performed in a double-blind manner without previous knowledge of the genotype by the person performing sectioning or counting.

Intraventricular infusion of IGF-1

Wild-type and 9-month-old *mnd/mnd* animals ($n = 5$ of each genotype) were deeply anesthetized with a mixture of 9% ketamine, 2.4% xylazine, and 1.25% acepromazine and stereotaxically implanted, as previously described (Holtzman et al., 1992), with a cannula to deliver either artificial CSF vehicle or IGF-1 (2 μ g/d for 7 d, obtained from Cephalon Inc.) via an Alzet minipump. After recovery from anesthesia, animals

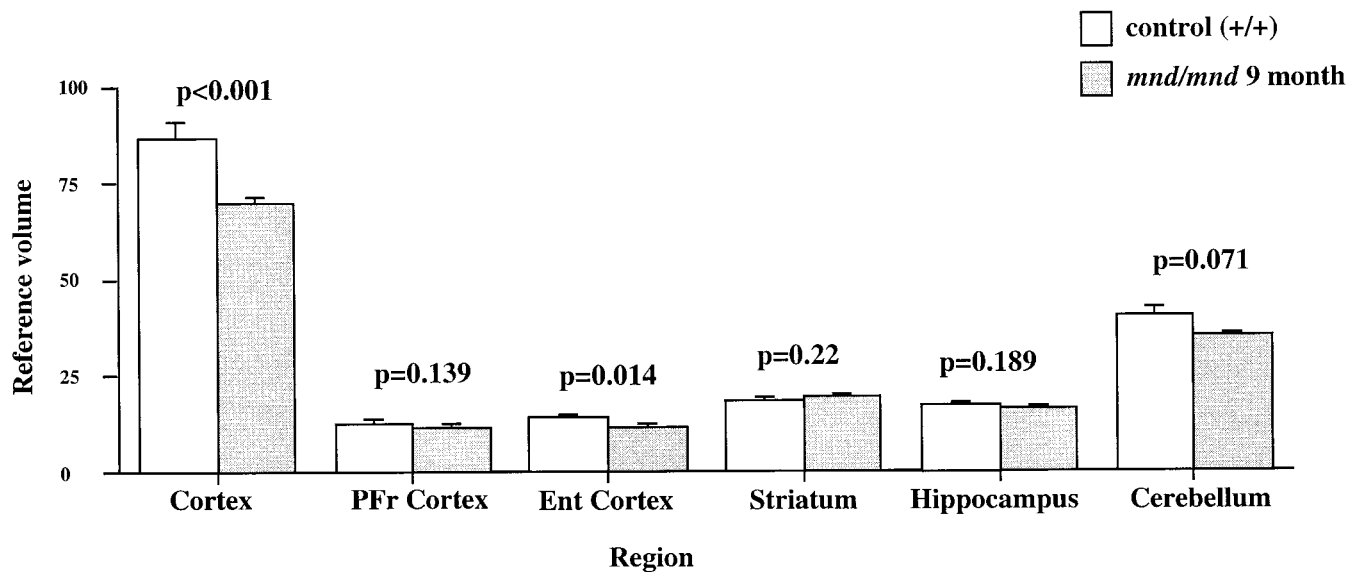


Figure 1. Reduction in neocortical volume in 9-month-old *mnd/mnd*. Unbiased estimates of the volume of different CNS regions were made by stereological point counting through the entire rostrocaudal extent of the CNS. The reference volume of the neocortical mantle was significantly reduced in 9-month-old *mnd/mnd*. Examination of cortical subregions revealed small, but significant, shrinkage of the entorhinal cortex (*Ent Cortex*) and cerebellum, but no change in the prefrontal cortex (*PFr Cortex*), striatum, or hippocampus.

were closely observed, and any animals showing signs of distress were removed from the study. After 7 d, animals were reanesthetized with pentobarbitone and fixed by transcardial perfusion as described above. Brains were subsequently removed, post-fixed, cryoprotected, and sectioned as described above. Animals with incorrect cannula placement were excluded from the study. Parallel series of sections through the hippocampal formation and entorhinal cortex were immunohistochemically stained to reveal the presence of PV, Cb, and SOM as described above. Measurements of histochemically identified interneuronal number and size were made in a double-blind manner as described above.

RESULTS

Aged *mnd/mnd* brains show cortical atrophy

Although *mnd/mnd* mice on the C57Bl/6J background show biochemical and pathological changes at 1 month of age, they are clinically healthy for ~6 months (Messer and Flaherty, 1986; Messer and Plummer, 1993). We compared the volume of different brain regions in *mnd/mnd* and control mice of the same strain at 5 (presymptomatic) and 9 months of age (severely weak). The Cavalieri method (1966) was used to obtain unbiased estimates of the volume of the cortical mantle, striatum, hippocampus, and cerebellum in Nissl-stained coronal sections. No significant difference was found in the volume of any brain region between control and *mnd/mnd* animals at 5 months (data not shown). However, at 9 months the volume of the neocortex in *mnd/mnd* mice was shrunken to 80.6% of the volume of age-matched controls (Fig. 1). Shrinkage was more pronounced in the entorhinal cortex than in the prefrontal cortex (Fig. 1), although significant shrinkage was evident in many regions of the neocortex. The cerebellum of 9-month-old *mnd/mnd* mice was also significantly smaller than in age-matched controls (Fig. 1). Detailed examination of the hippocampal formation of control and *mnd/mnd* mice at 5 months revealed no significant difference in the cross-sectional area of pyramidal neurons in region CA1: control, $95.18 \pm 0.52 \mu\text{m}^2$; *mnd/mnd*, $95.38 \pm 0.54 \mu\text{m}^2$; $n = 500$; $p = 0.79$; and no significant difference in the mean area of this region: control, $309343.74 \pm 14111.99 \mu\text{m}^2$; *mnd/mnd*, $322261.74 \pm 5454.93 \mu\text{m}^2$; $n = 5$; $p = 0.418$.

Progressive accumulation of autofluorescent lipopigment is most pronounced in presumed GABAergic neurons

We used the autofluorescent properties of the accumulated lipopigment to produce spatial and temporal maps of affected cells in the *mnd/mnd* mouse brain. Using conventional fluorescence microscopy, we examined unstained coronal sections throughout the rostrocaudal extent of the CNS of control and *mnd/mnd* mice at 2, 5, and 9 months. Consistent with previous reports, autofluorescent lipopigment could be detected in presymptomatic mutant mice at 2 months (Messer and Plummer, 1993). In contrast, autofluorescent lipopigment was almost entirely absent in age- and strain-matched wild-type animals of any age. By 5 months, lipopigment was present in many brain regions of mutant mice. Populations of lipopigment-bearing neurons could be readily identified in both cortical and subcortical regions. Prominent lipopigment accumulation was seen in midline neurons of the septal region, in several hippocampal subregions, throughout the neocortical mantle, in subregions of the basal ganglia, thalamus, and midbrain, and in cerebellum. Figure 2 compares control and *mnd/mnd* mice at 5 and 9 months. At both ages, autofluorescent lipopigment accumulation was marked in the septum and hippocampus of *mnd/mnd* mice. Immunohistochemical staining for subunit *c* of the mitochondrial ATPase showed that the distribution of subunit *c* deposits was the same as for lipopigment (data not shown). The distribution of autofluorescent lipopigment and its relative abundance were not dependent on the size of lipopigment-bearing neurons. Instead, at each age examined, lipopigment accumulation was particularly dense in populations of neurons presumed to be GABAergic on the basis of their distribution and morphology (Fig. 2). The distribution of lipopigment became progressively more widespread with increasing age until it was present in nearly all neurons of mutant mice at 9 months (data not shown). Qualitative comparisons revealed no obvious loss of neurons that were lipopigment-bearing in the septum or hippocampus between 5 and 9 months (Fig. 2).

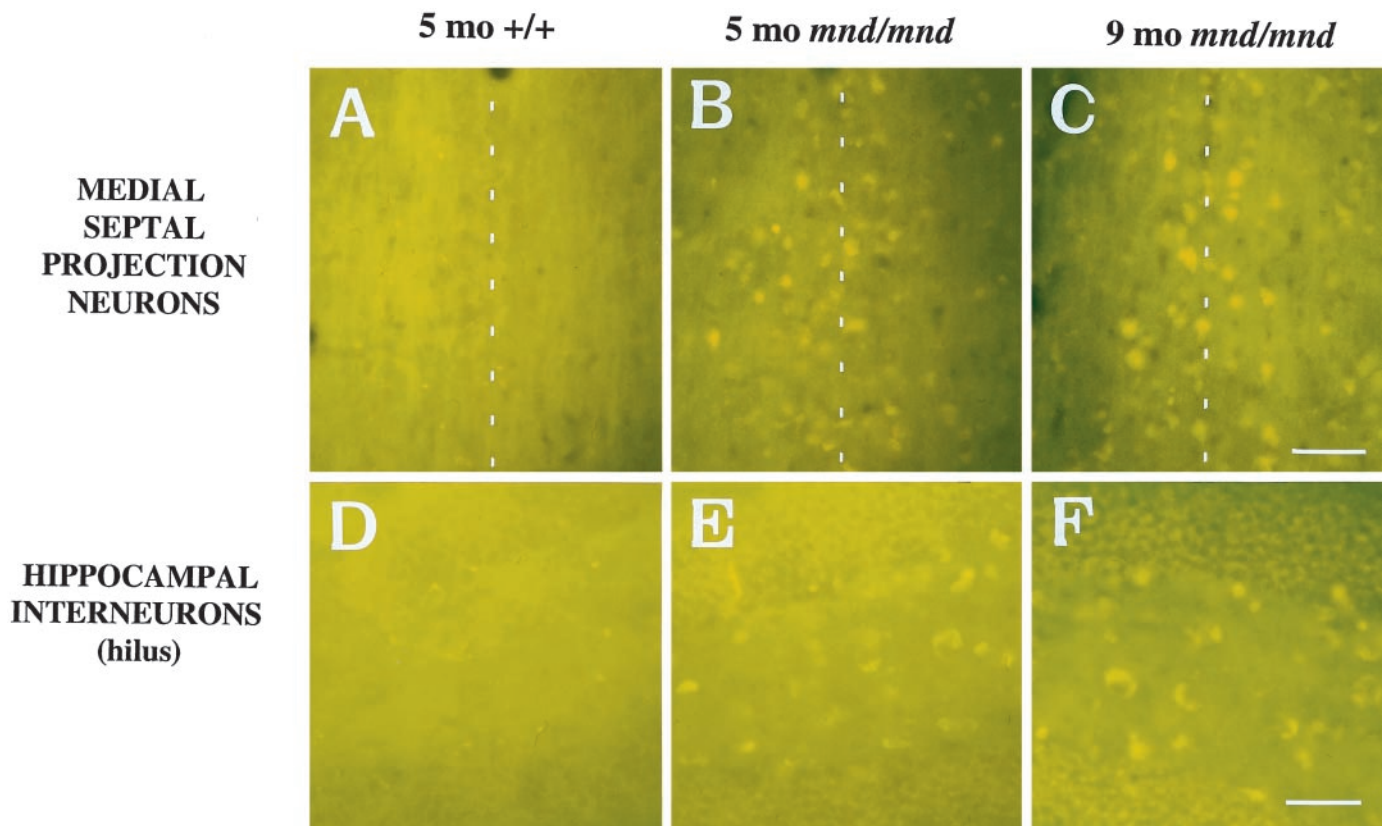


Figure 2. Presence of autofluorescent lipopigment in brains of *mnd/mnd* mice at 5 and 9 months. *A–F*, Representative photomicrographs of unstained coronal sections through the CNS of 5-month-old control (+/+) (*A, D*) and *mnd/mnd* mice at 5 (*B, E*) and 9 (*C, F*) months viewed by conventional fluorescence microscopy using an FITC filter set. Few scattered deposits of autofluorescent lipopigment are present in (+/+) mice. In 5-month-old *mnd/mnd* animals, dense accumulations of autofluorescent lipopigment are present in midline neurons of the medial septum (*B*) and in hilar interneurons of the hippocampus (*E*). In 9-month-old *mnd/mnd* animals, accumulation of lipopigment in these regions is more prominent with no obvious reduction in the number of lipopigment-bearing neurons. *Dashed line* in *A–C* indicates midline. Scale bars: *A–F*, 226 μm .

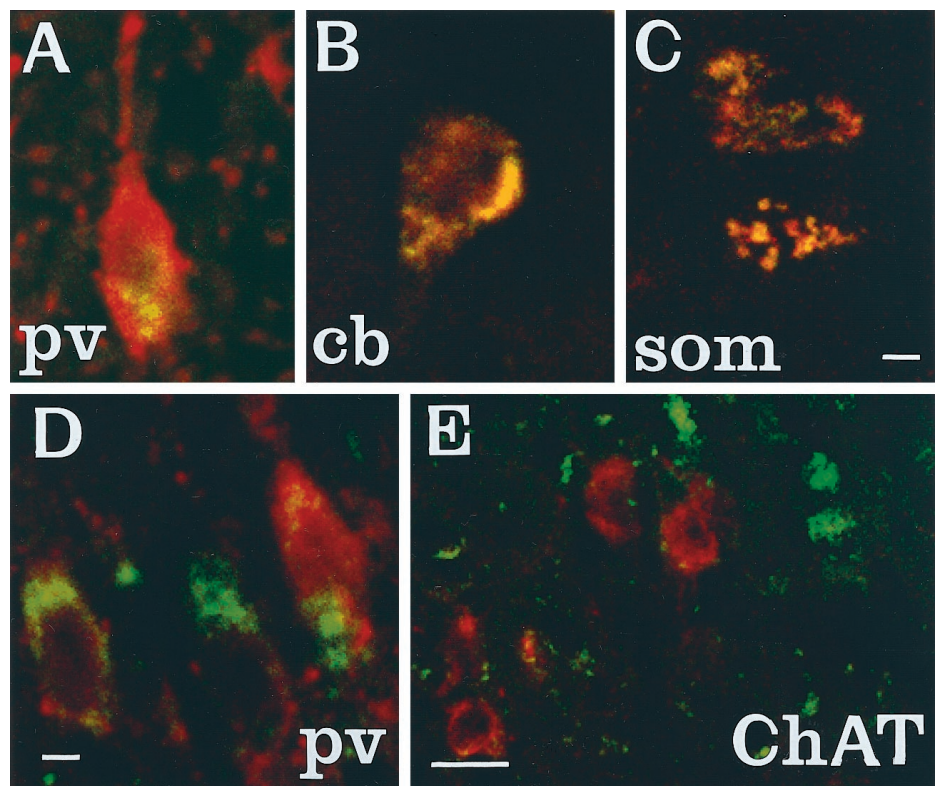


Figure 3. Colocalization of autofluorescent lipopigment with markers of interneuron phenotype. *A–E*, Representative photomicrographs of coronal sections through the hippocampus (*A–C*) and medial septum (*D, E*) of a 2-month-old *mnd/mnd* mouse viewed by confocal microscopy to reveal colocalization (yellow) of autofluorescent lipopigment (green) with markers of neuronal phenotype (red). *A*, Parvalbumin (*pv*)-positive neuron in stratum oriens adjacent to CA1. *B*, Calbindin (*cb*)-positive interneuron in stratum oriens adjacent to CA1. *C*, Somatostatin-14 (*som*)-positive hilar interneurons. *D*, Parvalbumin-positive medial septal neurons. *E*, Choline acetyltransferase (*ChAT*)-positive septal neurons (red) contain little lipopigment compared with adjacent midline parvalbumin-positive neurons (green). Scale bars: *A–D*, 12 μm ; *E*, 48 μm .

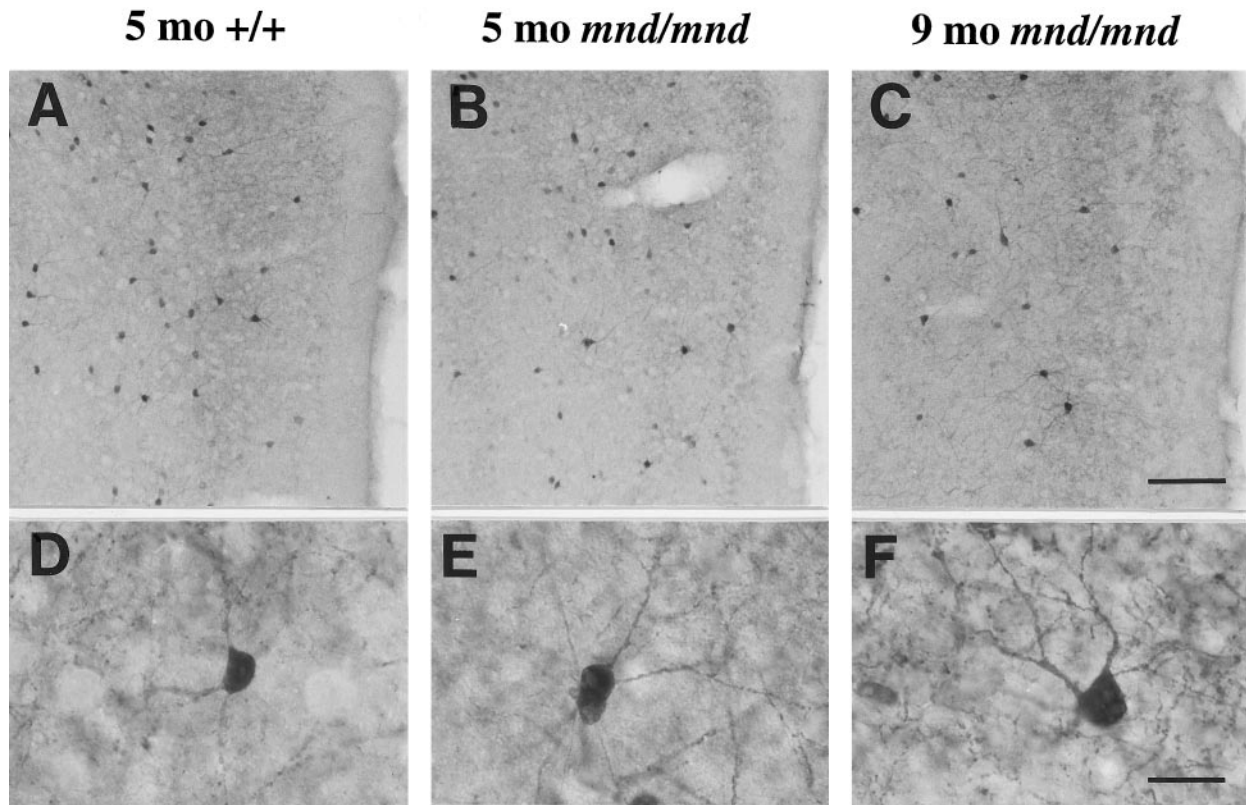


Figure 4. Progressive hypertrophy and loss of detectable parvalbumin-stained interneurons in the entorhinal cortex of *mnd/mnd* mice. Representative photomicrographs of parvalbumin-stained coronal sections of the entorhinal cortex of 5-month-old control (+/+) (*A, D*) and *mnd/mnd* mice at 5 (*B, E*) and 9 (*C, F*) months. *A–C*, Fewer parvalbumin-positive interneurons are apparent in laminae II and IV of 5-month-old *mnd/mnd* mice (*B*). This loss is more pronounced in mutant mice of 9 months (*C*). *D–F*, Higher power reveals that persisting neurons appear hypertrophic and exhibit thickened dendritic processes in aged *mnd/mnd* (*F*). Scale bars: *A–C*, 105 μ m; *D–F*, 22 μ m.

Accumulation of autofluorescent lipopigment in different subpopulations of interneurons

Fluorescence immunohistochemistry was used to identify which neuronal populations were affected. To determine the identity of those neurons that contained particularly dense accumulation of lipopigment, confocal microscopy was used for simultaneous visualization of lipopigment and cells stained with several different markers of neuronal phenotype (Fig. 3). Reliable staining of interneurons could not be obtained with commercially available antisera raised against GABA or its synthetic enzyme GAD which, even under optimal staining conditions, produced high levels of background staining that prevented distinct visualization of interneuronal morphology. However, interneurons were readily stained with antisera raised against the calcium-binding proteins PV or Cb and the neuropeptide SOM, that are each colocalized with GABA in many distinct subpopulations of GABAergic neurons (Freund and Buzsáki, 1996). PV and Cb have been suggested to modify or prevent neurodegenerative events in hippocampal neurons via their ability to buffer against increases in intracellular calcium concentration (Scharfman and Swartzkronin, 1989; Sloviter, 1989; Mattson et al., 1991). As such, changes in the expression of these proteins might mark neurons that are rendered more vulnerable to neurodegenerative processes. At 2 months, colocalization of lipopigment and these markers was detected by confocal microscopy in each region examined (Fig. 3). Representative examples of colocalization of lipopigment with PV, Cb, and SOM are shown in different subclasses of hippocampal interneurons and in the septal region (Fig.

3*A–D*). In contrast, neurons in adjacent regions stained with ChAT, a marker of cholinergic, (i.e., non-GABAergic) phenotype showed little or no autofluorescent lipopigment at this age (Fig. 3*E*). This analysis showed that lipopigment was present in subpopulations of GABAergic neurons throughout the rostrocaudal extent of the CNS. In all regions examined, neurons that expressed these GABA-associated markers showed prominent accumulation of autofluorescent lipopigment.

Progressive hypertrophy and loss of certain phenotypic markers in interneurons

To ask whether lipopigment accumulation marked neurons whose phenotype is affected during disease progression, we examined populations of PV-positive interneurons in the entorhinal cortex and subpopulations of PV-, Cb-, SOM-, and GAD-positive interneurons in the hippocampal formation.

Entorhinal cortex

Examination of the entorhinal cortex of *mnd/mnd* animals revealed a progressive loss of staining for PV in detectable interneurons in layers II and IV (Fig. 4*A–C*), with hypertrophy of remaining PV-positive interneurons (Fig. 4*D–F*). Counts of neuronal number revealed fewer than normal detectable PV-positive interneurons in layers II and IV of entorhinal cortex at 5 months, although this difference did not reach statistical significance, control, 48.35 ± 6.55 neurons per section; *mnd/mnd*, 37.41 ± 1.89 neurons per section; $p = 0.16$; $n = 4$ (Fig. 5*A*). Significantly fewer

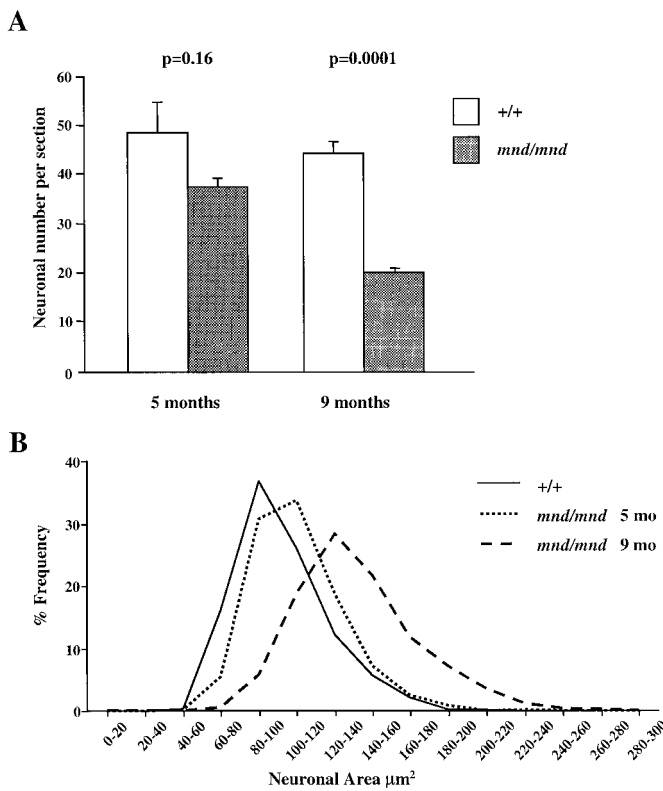


Figure 5. Number and size of detectable parvalbumin-stained interneurons in the entorhinal cortex of *mnd/mnd* mice. **A**, Histogram of Abercrombie-corrected number of detectable parvalbumin-positive interneurons per section of entorhinal cortex. Fewer parvalbumin-positive neurons were detected in *mnd/mnd* versus control (+/+) animals at 5 and 9 months, although this reduction in neuronal number was only significant in aged *mnd/mnd*. **B**, Plot of cell size distribution revealed hypertrophy of remaining parvalbumin-positive interneurons in *mnd/mnd* mice that was more pronounced in aged *mnd/mnd*.

PV-positive interneurons were detected at 9 months: control, 44.29 ± 2.46 neurons per section; *mnd/mnd*, 19.88 ± 0.96 neurons per section; $p = 0.0001$; $n = 5$ (Fig. 5A). Comparison of cross-sectional area revealed no significant change in the size of these neurons in 5-month-old mutant animals: control, $108.49 \pm 1.15 \mu\text{m}^2$; *mnd/mnd*, $110.35 \pm 1.21 \mu\text{m}^2$; $p = 0.266$; $n = 400$. However, hypertrophy was pronounced at 9 months: control, $102.7 \pm 1.08 \mu\text{m}^2$; *mnd/mnd*, $141.71 \pm 1.42 \mu\text{m}^2$; $p = 0.0001$; $n = 500$. The progressive nature of this hypertrophy was more clearly revealed by comparing cell-size distribution histograms at different ages (Fig. 5B). This analysis indicates that the increase in mean neuronal area cannot be explained simply by a loss of smaller PV-positive interneurons.

Hippocampus

Examination of the hippocampal formation of *mnd/mnd* animals revealed a complex pattern of progressive loss of staining for PV, Cb, or SOM in detectable subpopulations of hippocampal interneurons (Fig. 6). To survey these effects, counts of detectable neuronal number were made in each of the hippocampal subregions containing neurons positive for these antigens (Fig. 7, Table 1). Collectively, the results showed a consistent trend toward reduced neuronal number for each marker in all subregions at 5 months. However, the reduction in neuronal number reached statistical significance only for PV-positive interneurons in the dentate gyrus and stratum radiatum. In contrast, at 9 months significant reductions in neuronal number ($p < 0.0001$) were present in nearly all subregions and reached up to 87% in some populations. The only exception was Cb-positive interneurons in the stratum radiatum that showed no significant reduction in number at any age.

To examine expression of an essential marker of the neurotransmitter function of these interneurons, we stained a parallel series of sections through the hippocampal formation of control and *mnd/mnd* mice with an affinity-purified antiserum raised

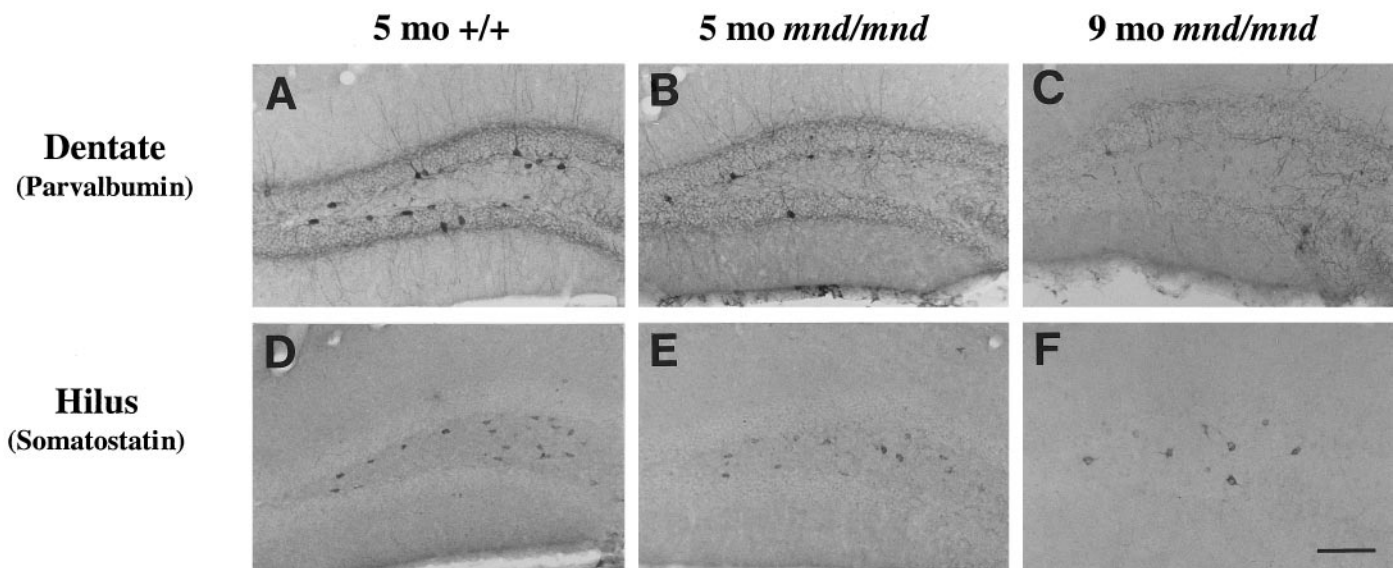


Figure 6. Loss of detectable interneurons in the hippocampus of *mnd/mnd* mice. **A–F**, Representative photomicrographs of coronal sections through the hippocampal formation of 5-month-old control (+/+) (**A**, **D**) and *mnd/mnd* mice at 5 (**B**, **E**) and 9 months (**C**, **F**) stained for parvalbumin (**A–C**) or somatostatin-14 (**D–F**). Note the progressive loss of detectable parvalbumin- and somatostatin-positive neurons. Remaining neurons exhibit progressive hypertrophy. Scale bar: **A–F**, 113 μm .

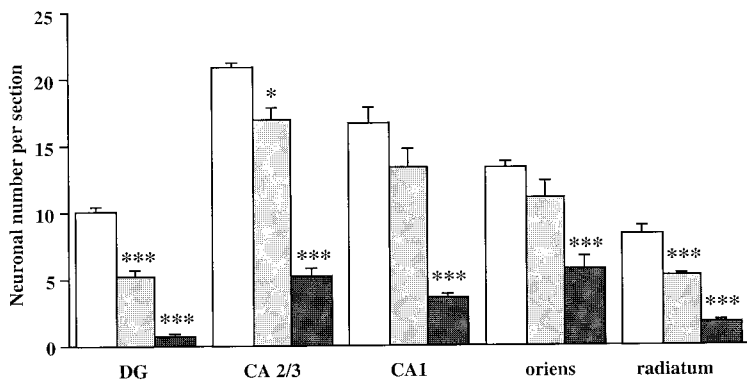
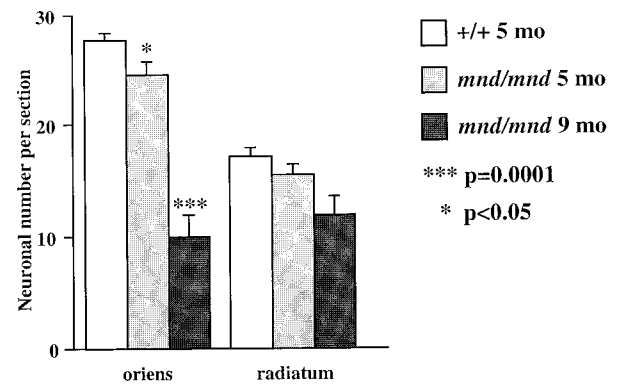
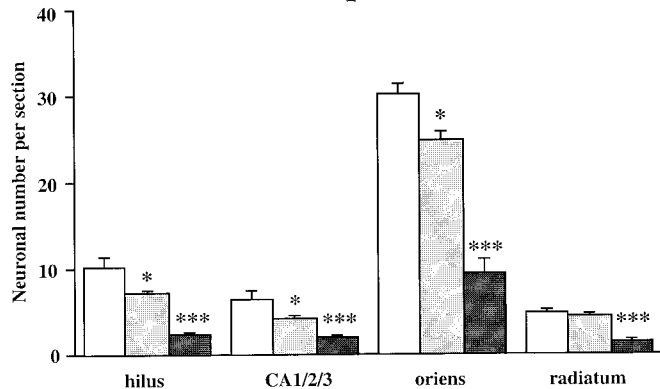
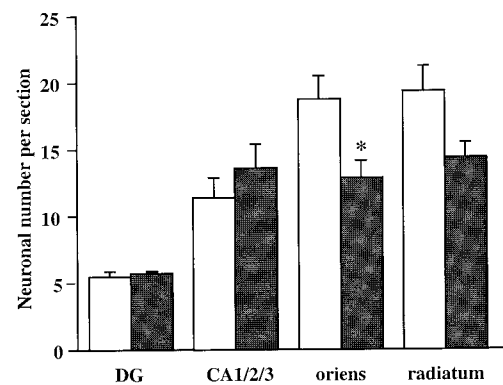
A. PARVALBUMIN positive**C. CALBINDIN positive****B. SOMATOSTATIN positive****D. GAD positive**

Figure 7. Loss of detectable interneurons in the hippocampus of *mnd/mnd* mice. *A–D*, Histograms of Abercrombie-corrected counts of detectable interneuronal number per coronal section through the hippocampal formation stained for parvalbumin (*A*), somatostatin-14 (*B*), calbindin (*C*), or glutamic acid decarboxylase (*D*). Loss of detectable parvalbumin-, calbindin-, or somatostatin-positive interneurons reached significance in almost every region by 9 months (*A–C*). In contrast, a significant change in glutamic acid decarboxylase-positive neuronal number was only seen in the stratum oriens at this age (*D*).

Table 1. Neuronal number

	Parvalbumin		Somatostatin		Calbindin		GAD
	5	9	5	9	5	9	9
Dentate	***	***	–	–	–	–	NS
Hilus	–	–	*	***	–	–	–
CA1	NS	***	–	–	–	–	–
CA2 + CA3	*	***	–	–	–	–	–
CA1 + CA2 + CA3	–	–	*	***	–	–	NS
Oriens	NS	***	*	***	*	***	*
Radiatum	***	***	NS	***	NS	NS	NS

Tabular representation of the relative statistical significance of changes in the number of detectable hippocampal interneurons stained for each antigen between control and mutant mice at 5 and 9 months in each region examined.

*** $p < 0.0001$; * $p < 0.05$; NS, not significant; –, not applicable.

against GAD (kindly provided by Dr. S. Baekkeskov, University of California, San Francisco) that, unlike commercially available antisera, enabled direct visualization of interneuronal morphology. Counts of neuronal number revealed no change in the number of GAD-positive neurons in the dentate or pyramidal cell layers in *mnd/mnd* mice at 9 months (Fig. 7). Although fewer

GAD-positive neurons were detected in other hippocampal regions of these *mnd/mnd* mice, the reductions in neuronal number only reached statistical significance in the stratum oriens: control, 18.63 ± 1.87 neurons per section; *mnd/mnd*, 12.82 ± 1.22 neurons per section; $n = 5$; $p = 0.044$. These reductions in interneuronal number are smaller than those detected by staining for PV, Cb, or SOM and suggest that the loss of interneurons detected by these other phenotypic markers are more apparent than real.

Closer examination of hippocampal sections revealed that persisting detectable interneurons in mutant mice appeared progressively larger with increasing age (Fig. 8). Neurons were grossly hypertrophic with characteristic enlargement of the axon hillock and thickening and disorganization of dendritic processes. Measurements of cross-sectional area (Table 2) revealed that at 5 months, eight of the 11 populations of interneurons examined were significantly larger than their counterparts in control animals. At 9 months, significant increases in cross-sectional area were apparent for each antigen in every region examined (Table 2). The population-wide nature of this hypertrophy and its progression over time were more clearly revealed by comparison of cell-size distribution histograms at different ages, as shown for a representative population of hippocampal interneurons (Fig. 8*D*).

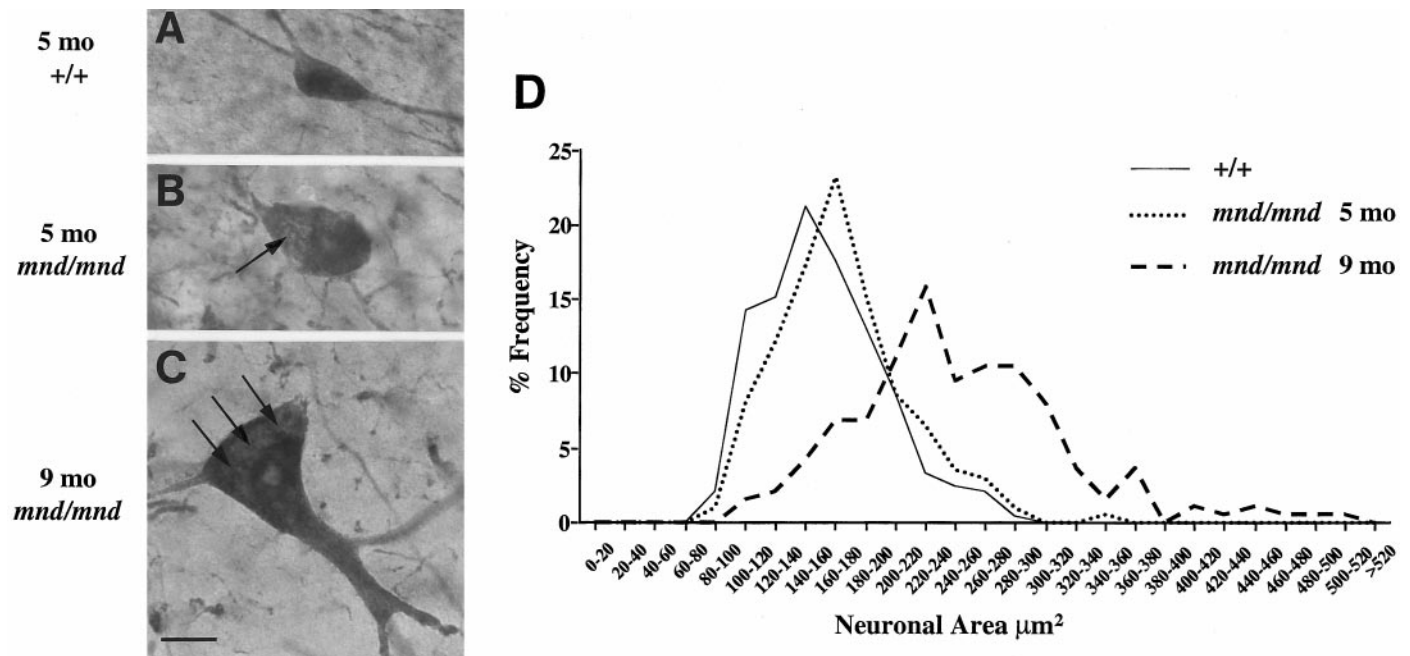


Figure 8. Progressive hypertrophy of hippocampal interneurons. *A–C*, Representative photomicrographs taken at the same magnification (100 \times objective) of parvalbumin-stained interneurons in the stratum oriens of control (+/+) (*A*) and *mnd/mnd* mice at 5 (*B*) and 9 (*C*) months. Note the progressive increase in soma size. *Arrows* indicate areas of reduced staining intensity that correspond to dense accumulations of storage material. Scale bar: *A–C*, 12 μ m. *D*, Plots of cell size distribution in a representative population of parvalbumin-positive interneurons revealed hypertrophy of persisting interneurons in *mnd/mnd* mice that was more pronounced in aged *mnd/mnd*.

Table 2. Neuronal area

	Parvalbumin		Somatostatin		Calbindin		GAD
	5	9	5	9	5	9	9
Dentate	*	***	–	–	–	–	***
Hilus	–	–	NS	***	–	–	–
CA1	NS	***	–	–	–	–	–
CA2 + CA3	***	***	–	–	–	–	–
CA1 + CA2 + CA3	–	–	***	***	–	–	***
Oriens	*	***	***	***	***	***	***
Radiatum	NS	***	*	***	***	***	***

**

Tabular representation of the relative statistical significance of changes in cross-sectional area of hippocampal interneurons stained for each antigen between control and mutant mice at 5 and 9 months in each region examined.

*** $p < 0.0001$; * $p < 0.05$; NS, not significant; –, not applicable.

Parvalbumin-positive projection neurons are not lost in *mnd/mnd* mice

To determine whether the effects on neuronal phenotype were specific to interneurons, we examined a representative population of GABAergic projection neurons in the medial septum that also accumulate lipopigment (Figs. 2, 3). These neurons send their efferent projections to the hippocampal formation where they terminate on different subclasses of inhibitory interneurons (Freund and Antal, 1988). The vast majority of medial septal GABAergic neurons contain parvalbumin, which is a good marker of GABAergic phenotype in this region (Freund, 1989; Kiss et al., 1990). Unbiased counts of neuronal number and neuronal size were made in control and *mnd/mnd* animals at 5 and 9 months using the optical dissector method in combination

with the Cavalieri method for estimating reference volume (West and Gundersen, 1990). There was no significant reduction in the number of PV-positive neurons in the medial septum of *mnd/mnd* mice at 5 months: control, 636.75 ± 24.58 ; *mnd/mnd*, 623 ± 43.11 ; $p = 0.791$; $n = 4$ (Fig. 9). However, these neurons were slightly, but consistently, larger in mutant mice than in age-matched controls: control, $120.91 \pm 1.15 \mu\text{m}^2$; *mnd/mnd*, $125.89 \pm 1.24 \mu\text{m}^2$; $p = 0.003$; $n = 500$. At 9 months, a difference in size was no longer apparent (control, $131.86 \pm 1.42 \mu\text{m}^2$; *mnd/mnd*, $132.16 \pm 1.53 \mu\text{m}^2$; $p = 0.88$; $n = 477$). No significant loss of detectable neurons was evident at 9 months. Indeed at this age, there was a significant increase in the number of PV-positive septal neurons in *mnd/mnd* mice: control, 591 ± 18.38 ; *mnd/mnd*, 711.6 ± 39.96 ; $p = 0.025$; $n = 5$ (Fig. 9).

Cholinergic neurons are found lateral to GABAergic neurons in the septal region and show little or no accumulation of autofluorescent lipopigment at 2 months (Fig. 3*E*). Neurons stained for the cholinergic neurotransmitter synthetic ChAT showed no significant change in unbiased estimates of detectable neuron number between *mnd/mnd* and wild-type mice at either 5 or 9 months (Fig. 9). However, these neurons were slightly but consistently larger in *mnd/mnd* mice at 9 months: control, $158.31 \pm 1.32 \mu\text{m}^2$; *mnd/mnd*, $166.16 \pm 1.43 \mu\text{m}^2$; $p = 0.0001$; $n = 600$. The reference volume of the septal region was not significantly different between control and mutant animals at any age in sections stained for PV or ChAT (data not shown).

Intraventricular infusion of IGF-1 partially reverses hippocampal interneuronal atrophy and loss

To test whether IGF-1 treatment could reverse pathology involving interneurons in *mnd/mnd* mice, we compared the effect of intracerebroventricular infusion with 2 $\mu\text{g/d}$ IGF-1 or artificial CSF vehicle. IGF-1 was previously shown to have beneficial effects on detectable GABAergic interneuronal number and den-

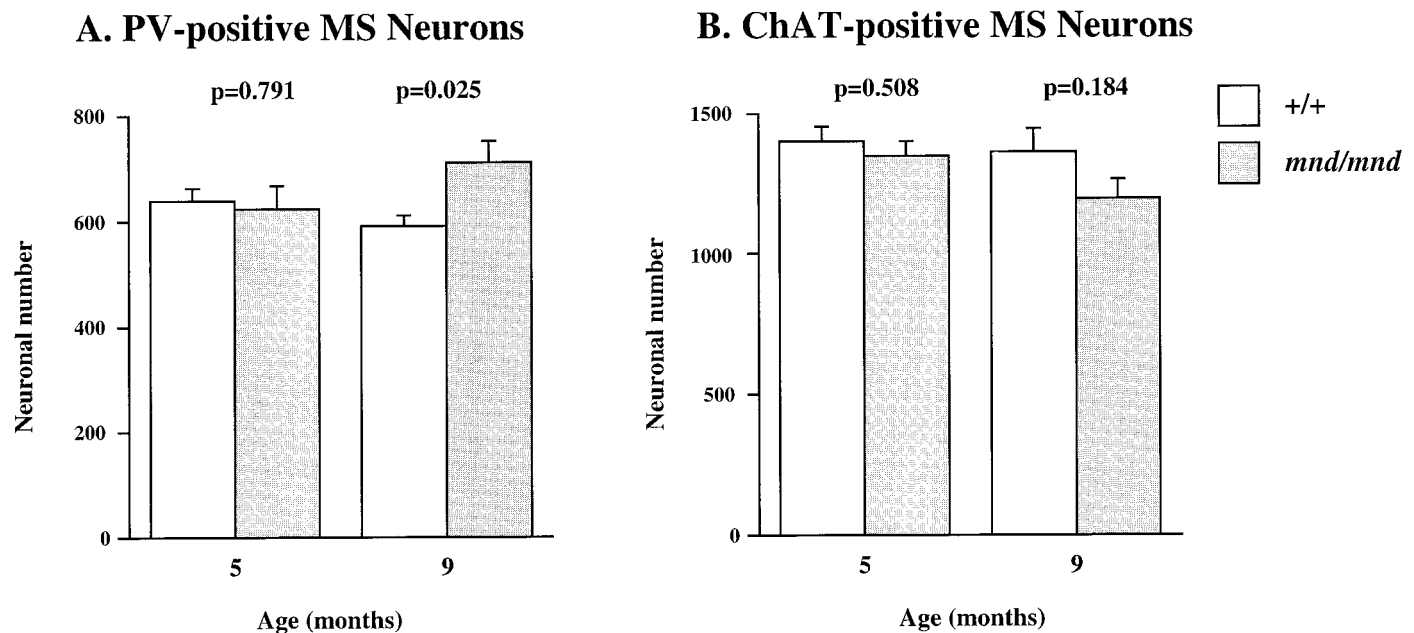


Figure 9. GABAergic projection neurons and cholinergic neurons are unaffected in the septal region of *mnd/mnd* mice. Histograms of unbiased stereological estimates of the detectable number of PV-positive (*A*) and ChAT-positive (*B*) neurons in the medial septum of control (+/+) and *mnd/mnd* mice at 5 and 9 months. No significant reduction in neuronal number was detected for either antigen at any age, although a significant increase in the number of parvalbumin-positive septal neurons was detected in aged *mnd/mnd*.

driftic morphology in a canine tissue culture model of NCL (Dunn et al., 1994). Nine-month-old control and *mnd/mnd* animals were perfused after 7 d of treatment, and analysis of interneuronal number in the entorhinal cortex and hippocampal formation was performed as described above.

Remarkably, treatment with IGF-1 significantly increased the number of SOM-positive hilar interneurons compared with age-matched, vehicle-treated mutant animals: vehicle, 1.79 ± 0.07 neurons per section; IGF-1, 2.48 ± 0.16 neurons per section; $n = 5$; $p = 0.012$ (Fig. 10*A*). Increases in interneuronal number in other subregions were found, but these changes did not reach statistical significance (representative example shown in Fig. 10*C*). The effect of IGF-1 treatment on cross-sectional area was more robust than the effect on neuronal number (Fig. 10*B,D*). IGF-1 treatment significantly reduced the size of SOM-positive hilar interneurons: vehicle, $219.77 \pm 4.79 \mu\text{m}^2$; IGF-1, $204.19 \pm 3.77 \mu\text{m}^2$; $n = 175$; $p = 0.011$; PV-positive interneurons in the stratum oriens: vehicle, $282.82 \pm 7.04 \mu\text{m}^2$; IGF-1, $263.37 \pm 6.85 \mu\text{m}^2$; $n = 186$; $p = 0.05$; and PV-positive interneurons of the dentate gyrus: vehicle, $296.70 \pm 17.88 \mu\text{m}^2$; IGF-1, $262.99 \pm 8.36 \mu\text{m}^2$; $n = 56$; $p = 0.056$. Despite this, we detected no obvious difference in IGF-1 treated animals in the density of lipopigment deposits in SOM- or PV-positive neuronal cell bodies or in the morphology of their dendrites. No significant effect was apparent for either interneuronal size or detectable number in the entorhinal cortex of IGF-1-treated mutant animals (data not shown). In addition, there was no effect of IGF-1 treatment on the number or size of any interneuronal population in the hippocampus or entorhinal cortex of control animals (data not shown).

DISCUSSION

In this study we used the autofluorescent properties of accumulated storage material to map which CNS neuronal populations in the *mnd/mnd* mouse show NCL-like pathological changes. We found a pronounced, early accumulation of autofluorescent lipop-

igment in subpopulations of GABAergic interneurons in the cortex and hippocampus. In these same cells there was loss of staining for some, but not all, phenotypic markers and pronounced hypertrophy of remaining detectable interneurons. Treatment with IGF-1 partially restored interneuronal number and reduced hypertrophy in some subregions. These results provide the first evidence for the involvement of interneurons in a mouse model of NCL. Moreover, our findings suggest that for at least some populations of these neurons, degenerative changes are growth factor-responsive.

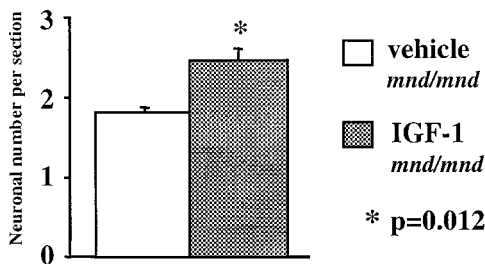
The *mnd/mnd* mouse as a model for NCL

The *mnd/mnd* mouse has been described previously as exhibiting a range of pathological features closely resembling those seen in patients with juvenile NCL (Bronson et al., 1993; Mazurkiewicz et al., 1993; Pardo et al., 1994). This mouse exhibits progressive retinopathy (Messer et al., 1993), widespread accumulation of autofluorescent lipopigment, which stains positive for subunit *c* of mitochondrial ATPase, and other pathological markers present in patients with NCL (Bronson et al., 1993; Messer and Plummer, 1993; Pardo et al., 1994). We also show that there is profound atrophy of the entire neocortical mantle, a characteristic hallmark of NCL (Braak and Braak, 1993).

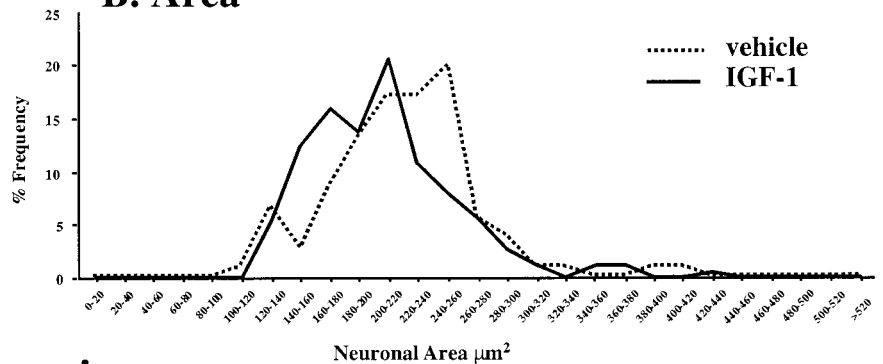
The identity of the mutated gene responsible for the phenotype of *mnd/mnd* mouse is unknown. Positional cloning has mapped the *mnd* gene to a proximal region of mouse chromosome 8 (Messer et al., 1992) and suggests that this gene locus is distinct from the genes CLN1, CLN2, and CLN3, which lie on other chromosomes. Nevertheless, ultrastructural analysis of cytoplasmic inclusions in the *mnd/mnd* mouse has revealed a range of granular, multilamellar, fingerprint, and curvilinear appearances, closely resembling those seen in patients with variant forms of late-infantile CLN2 (Pardo et al., 1994). Although the *mnd/mnd* mouse may model one of the late-infantile variant forms of NCL, the previously reported degeneration of motor neurons (Messer

SOMATOSTATIN positive hilus

A. Number

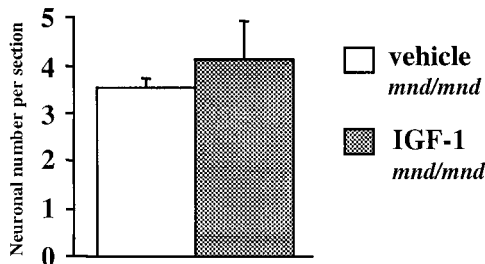


B. Area



PARVALBUMIN positive oriens

C. Number



D. Area

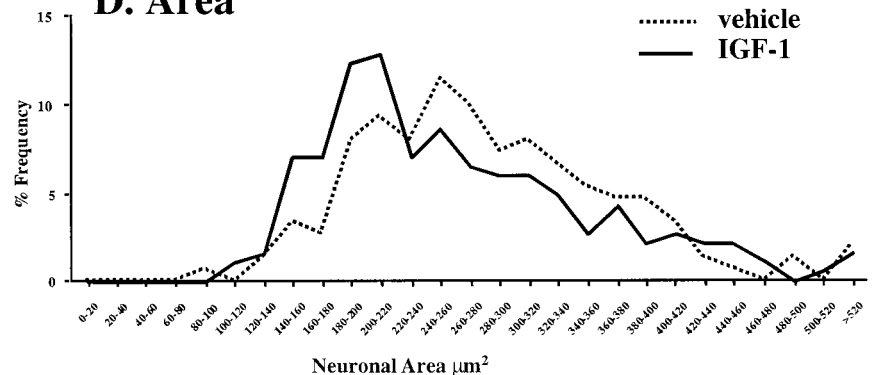


Figure 10. Partial recovery of interneuron phenotype after treatment of 9-month-old *mnd/mnd* mice with IGF-1. Histograms of Abercrombie-corrected counts of detectable neuronal number per section (*A, C*) and plots of cell size distribution (*B, D*) in the hilus and stratum oriens stained for somatostatin (*A, B*) and parvalbumin (*C, D*). A small, but statistically significant increase in detectable somatostatin-positive neuronal number was seen in the hilus (*A*), but not for parvalbumin-positive neurons in the stratum oriens (*C*). In contrast, significant reductions in neuronal hypertrophy were detected in both regions (*B, D*).

and Flaherty, 1986; Messer et al., 1987) emphasizes that this mouse cannot be considered a perfect model for NCL. Instead it represents an available mouse model of NCL-like pathology. Another spontaneous mutant, *nclf*, has recently been identified, which exhibits a grossly similar phenotype to the *mnd/mnd* mouse (Bronson et al., 1998). The *nclf* gene has been mapped to mouse chromosome 9 (Bronson et al., 1998), in a region syntenic to human chromosome 15q21 near the mapped locus for CLN6, another late infantile variant form of NCL (Sharp et al., 1997). Thus, *mnd* and *nclf* mice may both serve to model the pathology of rare variant forms of late-infantile NCL. It will be very informative to extend our studies to mice carrying null mutations in the genes associated with NCL, as these animals become available.

Involvement of interneurons in *mnd/mnd*

We detected novel evidence for the involvement of certain interneurons in the CNS of the *mnd/mnd* mouse. Although it remains unclear why lipopigment initially accumulates most prominently in subpopulations of GABAergic neurons, the literature contains several other reports of the involvement of these neurons in NCL (Walkley and March, 1993) and in other animal models of NCL (March et al., 1995). Previous studies of the neocortex of human NCL patients described a loss of small stellate neurons, which

were presumed to be GABAergic (Braak and Goebel, 1978, 1979), and a loss of ultrastructurally identified inhibitory synapses (Williams et al., 1977). Indeed, it has been suggested that a defect in inhibitory mechanisms may be responsible for generation of focal and generalized seizures in NCL (Roberts, 1986a,b). Recent evidence of the active role played by interneurons in information processing suggests that impairment of these neurons might also underlie the profound deficits in cognitive function that characterize the NCLs (for review, see Paulsen and Moser, 1998).

The selective involvement of GABAergic neurons in NCL and animal models may provide clues to pathogenesis. Mitochondrial abnormalities have been described in NCL patients (Dawson et al., 1996) and in a canine model of NCL (March et al., 1995). Mitochondria are more abundant in GABAergic neurons (Iversen and Bloom, 1972; Houser et al., 1984) and may also have different biochemical properties in these neurons that exhibit higher metabolic rates than other neuronal types. Compromised mitochondrial function in NCL, for whatever reason, might result in the preferential involvement of GABAergic neurons. However, it is unlikely that a mitochondrial defect operates in isolation to initiate NCL pathogenesis. Several lines of evidence suggest that lysosomal function is compromised. The genes CLN1 and CLN2,

which are mutated in the infantile and late infantile forms of the disorder, each code for a lysosomal enzyme (Vesa et al., 1995; Sleat et al., 1997). Additionally, recent evidence suggests that the CLN3 gene product is located in the lysosomal membrane and may function to regulate the transport of material into, or out of, the lysosome (Jarvela et al., 1998). Furthermore, findings in yeast suggest that the CLN3 homolog BTN1 plays a role in regulating the pH of a vacuolar lysosomal-equivalent compartment (Pearce and Sherman, 1998). A change in lysosomal pH may have profound effects on protein–protein interactions, resulting in the dysfunction of lysosomal enzymes.

In the hippocampal formation, the expression of calcium-binding proteins and neuropeptides is specific to different subtypes of interneurons, which show distinct patterns of connectivity (Freund and Buzsáki, 1996; Parra et al., 1998). Widespread changes in the expression of calcium-binding proteins might be expected to render these neurons more vulnerable to cell death via excitotoxic mechanisms (Choi, 1994).

Loss of detectable interneurons

Our findings demonstrate that in aged *mnd/mnd* mice progressively fewer GABAergic interneurons in both hippocampus and cortex can be detected by staining for markers that are normally present. The possibility arises that the reduction in number of immunohistochemically detected interneurons in the *mnd/mnd* mouse does not signify death but instead marks downregulation of these markers to the extent that they are no longer detectable. Indeed, we found that many interneurons retained expression of GAD in the hippocampal formation of aged *mnd/mnd* mice, suggesting that at least some populations of these neurons remain alive despite the absence of other normally expressed phenotypic markers. Further evidence for this hypothesis is our finding that treating aged *mnd/mnd* mice with IGF-1 increased the number in certain subpopulations of these neurons. Additional evidence for the persistence of interneurons comes from crude behavioral observation of seizure activity in *mnd/mnd* mice. Inhibitory interneurons in the hippocampus and cortex exert a powerful influence on excitatory transmission in these brain regions (Singer, 1996; Freund and Buzsáki, 1996). Although we did not carry out electrophysiological studies, we did not observe spontaneous seizures in *mnd/mnd* mice until at least 9 months, by which time up to 85% of PV-positive interneurons were not detected. Even at 9 months, seizures were evident clinically only occasionally. Thus, it is possible that a large proportion of GABAergic interneurons retain their inhibitory function even in severely affected animals.

Hypertrophy of cortical and hippocampal interneurons

We found that several subpopulations of interneurons were significantly larger in the *mnd/mnd* mouse than in controls. Neuronal volume regulation mechanisms remain largely unknown, and somal volume could be progressively increased in a number of ways. Dysfunction of mitochondrial respiration may result in inhibition of volume-regulated anion channels (Patel et al., 1998). Increased soma size may result from filling the cell cytoplasm with progressively increasing numbers of lysosomes or filling existing lysosomes to a greater extent. Each of these possibilities could profoundly influence neuronal function. Indeed, controlled shifts in lysosomal activity represent a means to regulate neuronal cytoplasmic volume and may potentially modify the function of a wide range of proteins, including neurotrophic signaling mechanisms (Nixon and Cataldo, 1995). The hypothesis that such mechanisms may be compromised in the *mnd/mnd* mouse awaits experimental verification.

Implications for the treatment of NCL

Treatment of 9-month-old *mnd/mnd* mice with IGF-1 partially restored interneuronal number and reduced hypertrophy in some subhippocampal subregions. It is remarkable that just 1 week of treatment was effective. These findings are evidence that at least some “phenotypically silent” neurons are growth factor-responsive. Indeed, IGF-1 treatment acted to reverse the neurodegenerative phenotype in responsive cells, suggesting that IGF-1 could have a role in therapy. However, IGF-1 treatment had no effect on the size or number of PV-positive interneurons in the entorhinal cortex, suggesting that other mechanisms may operate in this brain region, that degenerative changes had become irreversible before treatment was commenced, or that a longer course of treatment would be required to see an effect. It will be informative to test further the effect of IGF-1 and other neurotrophic factors, particularly at younger ages, to test whether a more robust effect in reversing the degenerative changes can be produced. Although our findings have direct implications for devising potential therapeutic strategies for the treatment of patients with NCL, rigorous tests of candidate strategies in appropriate animal models will be required.

REFERENCES

- Abercrombie M (1946) Estimation of nuclear populations from microtome sections. *Anat Rec* 94:239–247.
- Braak H, Braak E (1993) Pathoarchitectonic pattern of iso- and allo-cortical lesions in juvenile and adult neuronal ceroid-lipofuscinosis. *J Inherited Metab Dis* 16:259–262.
- Braak H, Goebel HH (1978) Loss of pigment-laden stellate cells: a severe alteration of the isocortex in juvenile neuronal ceroid lipofuscinosis. *Acta Neuropathol (Berl)* 42:53–57.
- Braak H, Goebel HH (1979) Pigmentoarchitectonic pathology of the isocortex in juvenile neuronal ceroid lipofuscinosis: axonal enlargements in layer IIIab and cell loss in layer V. *Acta Neuropathol (Berl)* 46:79–83.
- Bronson RT, Lake BD, Cook S, Taylor S, Davisson MT (1993) Motor neuron degeneration of mice is a model of neuronal ceroid lipofuscinosis (Batten's disease). *Ann Neurol* 33:381–385.
- Bronson RT, Donahue LR, Johnson KR, Tanner A, Lane PW, Faust JR (1998) Neuronal ceroid lipofuscinosis (*nclf*), a new disorder of the mouse linked to chromosome 9. *Am J Med Genet* 77:289–297.
- Cavalieri B (1966) *Geometria degli indivisibili*. Torino: Unione Tipografica, Editrice.
- Choi D (1994) Calcium and excitotoxic neuronal injury. *Ann NY Acad Sci* 747:162–171.
- Dawson G, Kilkus J, Siakotos AN, Singh I (1996) Mitochondrial abnormalities in CLN2 and CLN3 forms of Batten disease. *Mol Chem Neuropathol* 29:227–235.
- Dunn WA, Raizada MK, Vogt ES, Brown EA (1994) Growth factor-induced growth in primary neuronal cultures of dogs with neuronal ceroid lipofuscinosis. *Int J Dev Neurosci* 12:185–196.
- Dyken P (1988) Reconsideration of the classification of the neuronal ceroid lipofuscinoses. *Am J Med Genet [Suppl]* 5:69–84.
- Dyken P, Wisniewski K (1995) Classification of the neuronal ceroid-lipofuscinoses: expansion of the atypical forms. *Am J Med Genet* 57:150–154.
- Freund TF (1989) GABAergic septohippocampal neurons contain parvalbumin. *Brain Res* 478:375–381.
- Freund TF, Antal M (1988) GABA-containing neurons in the septum control inhibitory interneurons in the hippocampus. *Nature* 336:170–173.
- Freund TF, Buzsáki G (1996) Interneurons of the hippocampus. *Hippocampus* 6:347–470.
- Goebel HH (1995) The neuronal ceroid-lipofuscinoses. *J Child Neurol* 10:424–437.
- Goebel HH (1997) Morphologic diagnosis in neuronal ceroid lipofuscinosis. *Neuropediatrics* 28:167–169.
- Hall NA, Lake BD, Dewji NN, Patrick AD (1991) Lysosomal storage of subunit c of mitochondrial ATP synthase in Batten's disease (ceroid-lipofuscinosis). *Biochem J* 275:269–272.

- Haltia M, Rapola J, Santavuori P, Keranen A (1973) Infantile type of so-called neuronal ceroid-lipofuscinosis. 2. Morphological and biochemical studies. *J Neurol Sci* 18:269–285.
- Holtzman DM, Li Y, Parada LF, Kinsman S, Chen CK, Valletta JS, Zhou J, Long JB, Mobley WC (1992) p140trk mRNA marks NGF-responsive forebrain neurons: evidence that trk gene expression is induced by NGF. *Neuron* 9:465–478.
- Houser CR, Vaughan JE, Hendry SHC, Jones EG, Peters A (1984) GABA neurons in the cerebral cortex. In: *Cerebral cortex: functional properties of cortical cells*, Vol 2 (Jones EG, Peters A, eds), pp 63–89. New York: Plenum.
- The International Batten Disease Consortium (1995) Isolation of a novel gene underlying Batten disease, *CLN3*. *Cell* 82:949–957.
- Iverson LL, Bloom FE (1972) Studies of the uptake of ³H-GABA and [³H]glycine in slices and homogenates of rat brain and spinal cord by electron microscopic autoradiography. *Brain Res* 41:131–143.
- Jarvela I, Sainio M, Rantamaki T, Olkkonen VM, Carpen O, Peltonen L, Jalanko A (1998) Biosynthesis and intracellular targeting of the *CLN3* protein defective in Batten disease. *Hum Mol Genet* 7:85–90.
- Kiss J, Patel AJ, Freund TF (1990) Distribution of septohippocampal neurons containing parvalbumin or choline acetyltransferase in the rat brain. *J Comp Neurol* 298:362–372.
- Koenig H (1964) Neuronal lipofuscin in disease. Its relation to lysosomes. *Trans Am Neurol Assoc* 89:212–213.
- Kominami E, Ezaki J, Muno D, Ishido K, Ueno T, Wolfe LS (1992) Specific storage of subunit c of mitochondrial ATP synthase in lysosomes of neuronal ceroid lipofuscinosis (Batten's disease). *J Biochem* 111:278–282.
- March PA, Wurzelmann S, Walkley SU (1995) Morphological alterations in neocortical and cerebellar GABAergic neurons in a canine model of juvenile Batten disease. *Am J Med Genet* 57:204–212.
- Mattson MP, Rychlik B, Chu C, Christakos C (1991) Evidence for calcium-reducing and excitoprotective roles for the calcium-binding protein calbindin-D_{28K} in cultured hippocampal neurons. *Neuron* 9:943–954.
- Mazurkiewicz JE, Callahan LM, Swash M, Martin JE, Messer A (1993) Cytoplasmic inclusions in spinal neurons of the motor neuron degeneration (*Mnd*) mouse. *J Neurol Sci* 116:59–66.
- Messer A, Flaherty L (1986) Autosomal dominance in a late-onset motor neuron disease in the mouse. *J Neurogenet* 3:345–355.
- Messer A, Plummer J (1993) Accumulating autofluorescent material as a marker for early changes in the spinal cord of the *Mnd* mouse. *Neuromuscul Disord* 3:129–134.
- Messer A, Strominger NL, Mazurkiewicz JE (1987) Histopathology of the late-onset motor neuron degeneration (*Mnd*) mutant in the mouse. *J Neurogenet* 4:201–213.
- Messer A, Plummer J, Maskin P, Coffin JM, Frankel WN (1992) Mapping of the motor neuron degeneration (*Mnd*) gene, a mouse model of amyotrophic lateral sclerosis (ALS). *Genomics* 18:797–802.
- Messer A, Plummer J, Wong V, La Vail MM (1993) Retinal degeneration in motor neuron degeneration (*mnd*) mutant mice. *Exp Eye Res* 57:637–641.
- Nixon RA, Cataldo AM (1995) The endosomal-lysosomal system of neurons: new roles. *Trends Neurosci* 18:489–496.
- Palmer DN, Fearnley IM, Walker JE, Hall NA, Lake BD, Wolfe LS, Haltia M, Martinus RD, Jolly RD (1992) Mitochondrial ATP synthase subunit c storage in the ceroid-lipofuscinoses (Batten disease). *Am J Med Genet* 42:561–567.
- Pardo CA, Rabin BA, Palmer DN, Price DL (1994) Accumulation of the adenosine triphosphate synthase subunit C in the *mnd* mutant mouse. *Am J Pathol* 144:829–835.
- Parra P, Gulyás AI, Miles R (1998) How many subtypes of inhibitory cells in the hippocampus. *Neuron* 20:983–993.
- Patel AJ, Lauritzen I, Lazdunski M, Honoré H (1998) Disruption of mitochondrial respiration inhibits volume-regulated anion channels and provokes neuronal cell swelling. *J Neurosci* 18:3117–3123.
- Paulsen O, Moser EI (1998) A model of hippocampal memory encoding and retrieval: GABAergic control of synaptic plasticity. *Trends Neurosci* 21:273–278.
- Pearce DA, Sherman F (1998) A yeast model for the study of Batten disease. *Proc Natl Acad Sci USA* 95:6915–6918.
- Roberts E (1986a) Metabolic and nervous system disease: a challenge for our times. Part II. *Metab Brain Dis* 1:91–117.
- Roberts E (1986b) Failure of GABAergic inhibition: a key to local and global seizures. *Adv Neurol* 44:319–341.
- Santavuori P (1988) Neuronal ceroid lipofuscinosis in childhood. *Brain Dev* 10:80–83.
- Santavuori P, Rapola J, Nuutila A, Raininko R, Lappi M, Launes J, Herva R, Sainio K (1991) The spectrum of Jansky-Bielschowsky disease. *Neuropediatrics* 22:92–96.
- Savukoski M, Klockars T, Holmberg V, Santavuori P, Lander ES, Peltonen L (1998) *CLN5*, a novel gene encoding a putative transmembrane protein mutated in Finnish variant late infantile neuronal ceroid lipofuscinosis. *Nat Genet* 19:286–288.
- Scharfman HE, Schwartzkronin PA (1989) Protection of dentate hilar cells from prolonged stimulation by intracellular calcium chelation. *Science* 246:257–260.
- Sharp JD, Wheeler RB, Lake BD, Savukoski M, Jarvela J, Peltonen L, Gardiner RM, Williams RE (1997) Loci for classical and a variant late infantile neuronal ceroid lipofuscinosis map to chromosomal 11p15 and 15q21–23. *Hum Mol Genet* 6:591–596.
- Singer W (1996) Neurophysiology: the changing face of inhibition. *Curr Biol* 6:395–397.
- Sleat D, Donnelly RJ, Lackland H, Liu C-G, Sohar I, Pullarkat RK, Lobel P (1997) Association of mutations in a lysosomal protein with classical late-infantile neuronal ceroid lipofuscinosis. *Science* 277:1802–1805.
- Sloviter RS (1989) Calcium-binding protein (calbindin-D_{28K}) and parvalbumin immunocytochemistry: localization in the rat hippocampus with specific relevance to the selective vulnerability of hippocampal neurons to seizure activity. *J Comp Neurol* 280:183–196.
- Tyynelä J, Palmer DN, Baumann M, Haltia M (1993) Storage of saposins A and D in infantile neuronal ceroid-lipofuscinosis. *FEBS Lett* 330:8–12.
- Vesa J, Hellsten E, Verkruyse LA, Camp LA, Rapola J, Santavuori P, Hofmann SL, Peltonen L (1995) Mutations in the palmitoyl protein thioesterase gene causing infantile neuronal ceroid lipofuscinosis. *Nature* 376:584–587.
- Walkley SU, March PA (1993) Biology of neuronal dysfunction in storage disorders. *J Inher Metab Dis* 16:284–287.
- West MJ, Gundersen HJG (1990) Unbiased stereological estimation of the number of neurons in the human hippocampus. *J Comp Neurol* 231:482–497.
- Williams RS, Lott IT, Ferrante RJ, Caviness VS (1977) The cellular pathology of neuronal ceroid lipofuscinosis. *Arch Neurol* 34:298–305.